Cerebral Cortex, July 2020;30: 4011–4025

doi: 10.1093/cercor/bhaa017
Advance Access Publication Date: 28 February 2020
Original Article

ORIGINAL ARTICLE

Human Anterior Insula Encodes Performance Feedback and Relays Prediction Error to the Medial Prefrontal Cortex

Pablo Billeke[1], Tomas Ossandon[2,3], Marcela Perrone-Bertolotti[4,9], Philippe Kahane[5], Julien Bastin[6], Karim Jerbi[7,10,11], Jean-Philippe Lachaux[8] and Pablo Fuentealba[2]

[1]Laboratorio de Neurociencia Social y Neuromodulación, Centro de Investigación en Complejidad Social (neuroCICS), Facultad de Gobierno, Universidad del Desarrollo, Santiago CL 7610658, Chile, [2]Departamento de Psiquiatría, Facultad de Medicina y Centro Interdisciplinario de Neurociencia, Pontificia Universidad Católica de Chile, Santiago CL 8330024, Chile, [3]Institute of Biological and Medical Engineering, Pontificia Universidad Católica de Chile, Santiago CL 8330024, Chile, [4]Université Grenoble Alpes, CNRS, LPNC UMR 5105, Grenoble 38000, France, [5]Université Grenoble Alpes, Inserm, U1216, CHU Grenoble Alpes, Grenoble Institut Neurosciences, Grenoble 38000, France, [6]Université Grenoble Alpes, Inserm U1216, Grenoble Institut Neurosciences, Grenoble 38000, France, [7]Cognitive & Computational Neuroscience Lab, Psychology Department, University of Montreal, Montreal, QC H3T 1L5, Canada, [8]INSERM U1028, CNRS UMR5292, Brain Dynamics and Cognition Team, Lyon Neuroscience Research Center, Lyon, Bron 69004, France, [9]Institut Universitaire de France, [10]UNIQUE Research Center, QC, Canada, and [11]MILA (Quebec Artificial Intelligence Institute)

Address correspondence to Pablo Billeke, Laboratorio de Neurociencia Social y Neuromodulación, Centro de Investigación en Complejidad Social (neuroCICS), Facultad de Gobierno, Universidad del Desarrollo, Av. Las Condes 12461, Santiago CL-7610658, Chile. Email: pbilleke@udd.cl

Abstract

Adaptive behavior requires the comparison of outcome predictions with actual outcomes (e.g., performance feedback). This process of performance monitoring is computed by a distributed brain network comprising the medial prefrontal cortex (mPFC) and the anterior insular cortex (AIC). Despite being consistently co-activated during different tasks, the precise neuronal computations of each region and their interactions remain elusive. In order to assess the neural mechanism by which the AIC processes performance feedback, we recorded AIC electrophysiological activity in humans. We found that the AIC beta oscillations amplitude is modulated by the probability of performance feedback valence (positive or negative) given the context (task and condition difficulty). Furthermore, the valence of feedback was encoded by delta waves phase-modulating the power of beta oscillations. Finally, connectivity and causal analysis showed that beta oscillations relay feedback information signals to the mPFC. These results reveal that structured oscillatory activity in the anterior insula encodes performance feedback information, thus coordinating brain circuits related to reward-based learning.

Key words: beta oscillations, error monitoring, feedback, insula, intracortical recording

Introduction

Monitoring both the performance and outcomes of actions is fundamental for adapting behavior to challenging environmental conditions. During this monitoring, organisms compare internally generated predictions with actual outcomes in order to compute prediction error signals which are crucial for reward-based learning (Glimcher 2011). Several brain areas have been related to these monitoring performance processes. In particular, medial prefrontal cortical regions, such as the supplementary motor area (SMA) and the dorsal anterior cingulate cortex (dACC), play a pivotal role in detecting conflicts and errors to fix ongoing behavior and allocate cognitive resources to adapt subsequent behavior (Alexander and Brown 2011; Bonini et al. 2014; Shenhav et al. 2014; Billeke et al. 2014b). These areas are the main cortical target of mesolimbic dopaminergic neurons signaling prediction errors during reinforcement learning (Mark Williams and Goldman-Rakic 1998). Recent evidence from animal and human studies shows that there is an extended network of cortical areas that also respond to performance feedback (Ullsperger et al. 2014). One of these areas is the anterior segment of the insular cortex (AIC), which is in close functional and anatomical relationship with medial prefrontal regions (Dosenbach et al. 2007; Nelson et al. 2010; Power et al. 2011). In spite of the consistent co-activation between AIC and dACC in response to performance feedback, there is no consensus for the specific role played by the AIC in performance monitoring.

A line of evidence suggests that the AIC's involvement in performance monitoring may pertain to its role in error awareness (Klein et al. 2013). This view is supported by neuroimaging evidence showing robust AIC activation evoked by error or negative performance feedback (Ullsperger and von Cramon 2003; Dosenbach et al. 2006; Ham et al. 2013). Since AIC is known to be involved in interoception (Craig 2009), it is conceivable that it activates as a result of enhanced awareness to an autonomic reaction to an error (Klein et al. 2007). Nonetheless, when the valence of the feedback is controlled for frequency, both dACC and AIC seem to respond to the unexpectedness of the feedback valence rather than error per se (Ferdinand and Opitz 2014). This suggests that AIC activity cannot entirely be explained on the basis of error processing. Indeed, AIC-dACC network activations have been reported in several types of tasks (Dosenbach et al. 2006), indicating a general-purpose function related to the maintenance and implementation of task sets, as well as the coordination of behavioral responses (Medford and Critchley 2010). Another prevalent hypothesis suggests that dACC and AIC make-up a "salience network," highlighting their response to behaviorally relevant events (Seeley et al. 2007; Menon and Uddin 2010), but not novelty per se (Wessel et al. 2012). In this context, saliency can be understood as the property that characterizes the extent by which a stimulus deviates from the prediction, whether it surpasses it or falls short from it (i.e., unsigned prediction error). Interestingly, recent functional magnetic resonance imaging (fMRI) studies suggest that the AIC might be a central hub in cognitive processing since it exerts influence on the activity of other brain areas related to cognitive control and attention, including the medial prefrontal cortices (Sridharan et al. 2008; Higo et al. 2011; Ham et al. 2013).

Thus, despite a fair amount of evidence for the AIC involvement in performance monitoring, and its interaction with other cortical areas, the precise neuronal computations carried out in the AIC and the information flow to/from other key areas during performance monitoring remain poorly understood. Since previous studies using direct recordings from the human brain have demonstrated its strong potential in probing the electrophysiological underpinnings of performance monitoring (Jung et al. 2010, 2011; Bonini et al. 2014; Bastin et al. 2016), we recorded electrical brain activity from neurosurgical epileptic patients with intracerebral depth electrodes placed in the insular cortex for presurgical evaluation while they carried out various cognitive tasks with performance feedback. We tested the hypothesis that the AIC encodes performance feedback in order to adapt ongoing behavior to environmental conditions. In particular, we predicted that the electrophysiological activity of the AIC is modulated by the probability of the feedback valence and that it exerts a causal influence on other cortical areas related to feedback processing and reward-based learning, such as the medial prefrontal region (Sridharan et al. 2008; Ham et al. 2013).

We found robust oscillatory activity in the beta frequency range that was related to feedback processing in the electrodes located in the AIC. Remarkably, the power of beta oscillations was dynamically modulated by the expectancy of feedback valence (i.e., unsigned prediction error) in both between-task and within-task analyses. In addition, beta oscillations were nested in delta oscillations and presented a phase preference that encoded feedback valence. Finally, beta oscillations in the AIC influenced causally the activity of other cortical areas that showed feedback response, including medial prefrontal regions. The single-trial variation of the AIC influence on the medial prefrontal region correlated with the prediction error of feedback valence. Then, our results provide novel evidence for the critical role played by the AIC in the neural network that mediates the processing of performance feedback. Importantly, to the best of our knowledge, our findings are the first to reveal and characterize the transmission of performance monitoring signals from the AIC to medial prefrontal regions in humans.

Methods

Participants

Intracranial recordings were obtained from 19 epileptic patients (12 female, 17 right-handed) with intractable epilepsy who underwent stereotactic intracerebral EEG (SEEG) recordings before surgery at the Neurology Department of the Grenoble University Hospital (Grenoble, France). Patients' age was between 14 and 50 years (mean: 29.5) with an age of seizure onset ranging from 1 to 20 years (mean: 11 years). The implantation decision was only a guide for clinical aim. All electrode data presenting pathological waveforms were discarded from the present study. This procedure was achieved in collaboration with the medical staff. It was based on the visual inspection of the recordings and by systematically excluding data from any electrode sites that were found a posteriori to be located within the seizure onset zone (see Supplementary Table 1 for a complete description of the epileptic zone for each patient). All participants provided written informed consent, and the experimental procedures were approved by the local Ethical Committee ("ISD et SEEG" project, CPP Sud-Est V no 09-CHU-12).

Electrode Implantation

Eleven to 15 semi-rigid, multilead electrodes were stereotactically implanted in each patient. Each electrode had a diameter of 0.8 mm, and depending on the target structure, comprised 10–15 contact leads 2-mm wide and 1.5 mm apart (DIXI Medical). Electrodes were anatomically localized by aligning the pre-operative with the postoperative (i.e., electrodes in place) structural MRIs of each patient, and the localization was provided in MNI coordinates after normalization.

Experimental Tasks

We analyzed five different tasks. These tasks were selected given that all of them presented visual stimuli that indicated the performance of the subject in a given trial (performance feedback). The first two were designed for research purposes only, with the rationale that the probability of possible valence of the feedback was obtained by the subject explicitly (probabilistic decision-making [PDM]) or by learning (social decision-making [SDM] task, see below). The other tasks (a reading task and two working memory task) were selected from a pool of tasks used as the functional localizers of basic cognitive function in order to inform the presurgical decisions in a clinical setting. In these three tasks, the feedback valence is dependent on the performance of each patient. Thus, the probability of feedback valence depends on both individual performance and the difficulty of each condition (see below). Overall, all the tasks present performance feedback, but the source by which the subject can anticipate the probability of the specific valence differs across the tasks, allowing us the opportunity to study the consistent feedback processing independent of the specific task features or demands. The description of each task is the following:

1. PDM task (Supplementary Fig. 1). Patients had to decide between two probabilistic rewarded options. Each option was represented by the colors of the bar (on each side of the screen) and was associated with a probability of being selected, represented by the length of the colored bar placed in the center of the screen; and a payoff, represented by a number placed over each colored bar. The options had random, complementary probabilities and payoffs. The option with the highest probability had the lowest payoff, and vice versa. After the patient had chosen an option (1–3 s), the rewarded option was indicated with either a green circle in case the patient chose correctly or with a red circle otherwise. Feedback presentation (red or green circle) lasted 1 s. If the patient chose the rewarded option, he/she obtained the associated payoff. Otherwise, he/she received no money.
2. SDM task (Supplementary Fig. 2). We used a repeated version of the Ultimatum Game used in prior work (Billeke et al. 2013). In brief, patients played as proposers and had to make an offer to the other player (the responder) as how to split an amount of money (10 Euros) between them. The responder could either accept or reject the offer. If the offer is accepted, the money is split as proposed. While if the offer is rejected, none of the players received any money. Each game consisted of 30 consecutive rounds between the same pair of players. Patients believed they were playing with another human, but they were actually playing with a computational simulation that generated a credible social interaction (Billeke et al. 2014b). The feedback was a symbol indicating the responders' decisions (1 s). In the preceding two tasks (PDM and SDM tasks), the patients played for a symbolic reward and, hence, did not receive real money for their participation.
3. Reading task (RdT, Supplementary Fig. 3, Vidal et al. 2011). Patients saw a string of characters on the screen under three conditions. A word condition (semantic), where patients had to discriminate whether the word was referring to a living or nonliving object. A pseudo-word condition (phonologic), where patients had to discriminate whether the string had one or two syllables. Finally, a no-word condition (visual control), where patients had to discriminate whether the string consisted of uppercase or lowercase letters. After a trial, the feedback was shown indicating her/his performance (1.5 s).
4. Spatial working memory task (sWM, Hamamé et al. 2012). Patients had to memorize the positions of dots placed in a 4×4 array on the screen (2, 4, or 6 dots). After a pause, consisting of an empty array (3 s), a new dot was shown on it. Patients had to indicate whether the place of the new dot was filled or empty in the preceding array. After each trial, feedback indicated her/his performance (1.5 s).
5. Verbal working memory task (vWM, Hamamé et al. 2012). We used the Stemberg's task. Patients had to memorize letters (2, 4, or 6 letters). After a pause, consisting of a black screen (3 s), a new letter was shown, and the patient had to indicate whether the new letter appeared in the preceding strings. After each trial, feedback indicated her/his performance (1.5 s).

For all tasks, the time window of analysis was aligned with the apparition of the screen that indicated performance feedback (not the subjects' responses). All tasks were programmed in Presentation software (www.neurobs.com), and the responses were delivered through a gamepad using two buttons (using one hand for sWM, vWM, and RdT tasks and two hands for PDM and SDM tasks).

SEEG Recordings

Intracerebral electrical activity was recorded from 128 depth-EEG electrode sites using a video-EEG monitoring system (Micromed). Data were bandpass-filtered online (0.1–200 Hz) and sampled at 512 Hz. At the time of the acquisition, data were recorded using a reference electrode located within the white matter. Each electrode channel was rereferenced in respect to its closest neighbor (i.e., bipolar derivation). This bipolar montage had several advantages over standard referencing. It helped eliminate signal artifacts common to adjacent electrode contacts (such as the 50-Hz artifact or volumetric conductance of distant sources). It achieved a high local specificity by canceling out the effects of distant sources that spread equally to both adjacent sites through volume conduction. The spatial resolution achieved by bipolar SEEG recordings was of the order of 3 mm (Jerbi et al. 2009).

Electrode Localization

The electrodes were anatomically localized using the individual structural MRI postelectrode resection. Each MRI was co-registered to a standard MNI space, and the resulted coordinates were evaluated using an anatomical atlas provided by xjview 8 (http://www.alivelearn.net/xjview8). For insular cortex parcellation, we used the division suggested by Jakab et al. (2012) between the anterior and posterior parts. For the connectivity analysis between anterior insular cortex (AIC) and medial

prefrontal cortex (mPFC), we used a selected electrode in insular cortex per subject (the electrode with the higher responses) and all the electrodes whose nearest gray matter were located in medial part for frontal cortex, including the orbitofrontal cortex, and part of paracentral lobe and cingulate gyrus (anterior to coordinate MNI y = −32).

Time–Frequency Analysis

We computed time–frequency decomposition over continuous data using a wavelet transform. A signal x(t) was convolved with a complex Morlet's wavelet function defined by $w(t,f_0) = Ae^{-t^2/2\sigma_t^2}e^{i2\pi f_0 t}$. Wavelets were normalized, thus $A = (\sigma_t\sqrt{\pi})^{-1/2}$. The width of each wavelet function $m = f_0/\sigma_t$ was chosen to be 7, where $\sigma_f = \frac{1}{2}\pi\sigma_t$. Now time–frequency content was represented as the energy of the convolved signal $E(t,f_0) = |w(t,f_0) \otimes x(t)|^2$. For the presentation of continuous data, the time–frequency representation (TFR) was z-normalized using mean and standard deviation (SD) of the entire signal per electrode and frequency (Fig. 1). For the segmented TFR evoked feedback, we used a z-normalization related to a baseline period 1 s before feedback presentation. For the analysis of the power time course (alpha, beta, and gamma ranges), we used the Hilbert transform. Using a zero-phase shift noncausal finite impulse filter with 0.5-Hz roll-off, the continuous signals were first bandpass filtered in the frequency bands of interest (alpha 5–15 Hz, beta 15–30 Hz, and gamma 40–100 Hz). Now for each bandpass-filtered signal, we computed the envelope using the standard Hilbert transform. Finally, we z-normalized the resulting envelope related to a baseline period 1 s before the stimulus.

FT Statistical Analysis

For TFRs, we used the z-normalized signal related to baseline. We tested per each site (time × frequency bin) whether the means were other than zero using Wilcoxon signed-rank test.

For the analysis of the frequency band of interest, we used the z-normalized Hilbert envelope of the segmented signal of both feedback and control stimulus presentation. For group analysis, for both TFR and frequency band of interest, we first fitted a general linear model (GLM) per each electrode. For each bin (time × frequency), we computed a GLM using the following model:

$$E(t) = \beta_0 + \beta_1 F + \beta_2 V$$

where $E(t)$ is the z-normalized power of the frequency (form Wavelet transform) or envelop of the signal (from Hilbert transform), β_0 is the intercept of the model that represents the common activation related to feedback and control stimulus (see below), β_1 is the estimated slope of the feedback F representing the specific activation related to feedback (i.e., increases or decreases related to control stimulus), and β_2 is the estimated slope of the valence V (negative feedback = 1) representing the difference between negative and positive feedback (a negative slope indicates more activity for positive feedback and vice versa). Thus, each bin had an estimated slope and P-value per regressor. The control stimulus used in the model was different for the different tasks. For the PDM task, we used the appearance of the options, for the SDM the beginning of the decision period, for the RdT the presentation of the strings, and for the sWM and vWM we used the presentation of the stimuli to be memorized.

For the entire time/frequency series, we corrected the P-value using two approaches. For all analyses that have less than 30 observations (e.g., group analysis with less than 30 electrodes), we corrected using cluster-based permutation test (see below, cluster threshold detection $P < 0.01$, cluster corrected $P < 0.01$) and FDR $q < 0.01$ otherwise. The rationale of these approaches is trying to maintain a similar rate of both false positive but also false negative.

For the analysis of frequency band of interest, we say that an electrode is feedback and/or valence modulated if it has a significant modulation (corrected $P < 0.01$) for at least 50 ms.

For the correlation between task difficulty and beta activity, we selected the electrode within the AIC, having the highest response per subject in RdT task (the mean of the t-values during the 200 ms for which the maximum significant modulation was found). The difficulty of each task was estimated per each patient using the percentage of error. Then, the data (both error rate and beta responses) were rank transformed per each electrode, to avoid differences given by different electrode exposition. We used both the nonparametric Spearman correlation and the mixed linear model using random effect in the intercept and slope. In the latter approach, we used patients and tasks as grouping factor, in order to control the variance due to the difference in the electrode locations among patients. For these analyses, we tested the activity related to both the feedback and the valence. For the trial-by-trial correlation, we used the electrodes with the highest feedback response per patient. We used the mean during the 200 ms around the points of the maximum modulation per task in order to compute the power per trial. Thus, we correlated the power with the possibility to obtain positive feedback. This probability was estimated with different parameters for each task. For the PDM task, we used the logit transform of the probability of winning given by the colored area associated with the chosen option (explicitly given to the subject during the task). For the SDM task, we used the logit transform of the probability of obtaining an acceptance (given by the simulation, and learning by the subject across the task, for more details see prior work (Billeke et al. 2013, 2014a, 2014b, 2015; Melloni et al. 2016)). For the RdT, we used the difficulty of the three conditions given above (difficulty order: no-word condition < pseudo-word condition < word condition). Finally, for the memory tasks (vWM and sWM tasks), we used the number of items to keep in memory. In all these trial-by-trial correlations, we used both the nonparametric Spearman correlation and linear robust regression. Additionally, for a group analysis, we assessed if the rho value for all AIC electrodes and tasks presented positive or negative modulation by testing the mean of the rho value against zero. For this, we used the sign rank Wilcoxon test.

Phase–Amplitude Coupling

For a given frequency pair, the raw signal was filtered separately in both frequencies (zero phase shift noncausal finite impulse filter with 0.5 Hz roll-off). Lower frequency ranges from 0.5 to 35 Hz, (0.4 Hz increments, 0.8-Hz filtered bandwidth), and the higher ranged from 5 to 120 Hz (1 Hz increments, 5-Hz filtered bandwidth). The phase of the lower and the amplitude of the higher frequency range were computed using the Hilbert transform. For each epoch of interest (0–1 s after feedback for feedback processing and −1 to 0 s before feedback for baseline period), we computed the circular-linear correlation between the phase of lower frequencies and the amplitude of higher frequencies, and then we computed the mean per electrode. At group level analysis, per each frequency pair, we compared if the correlation coefficient was statistically different between

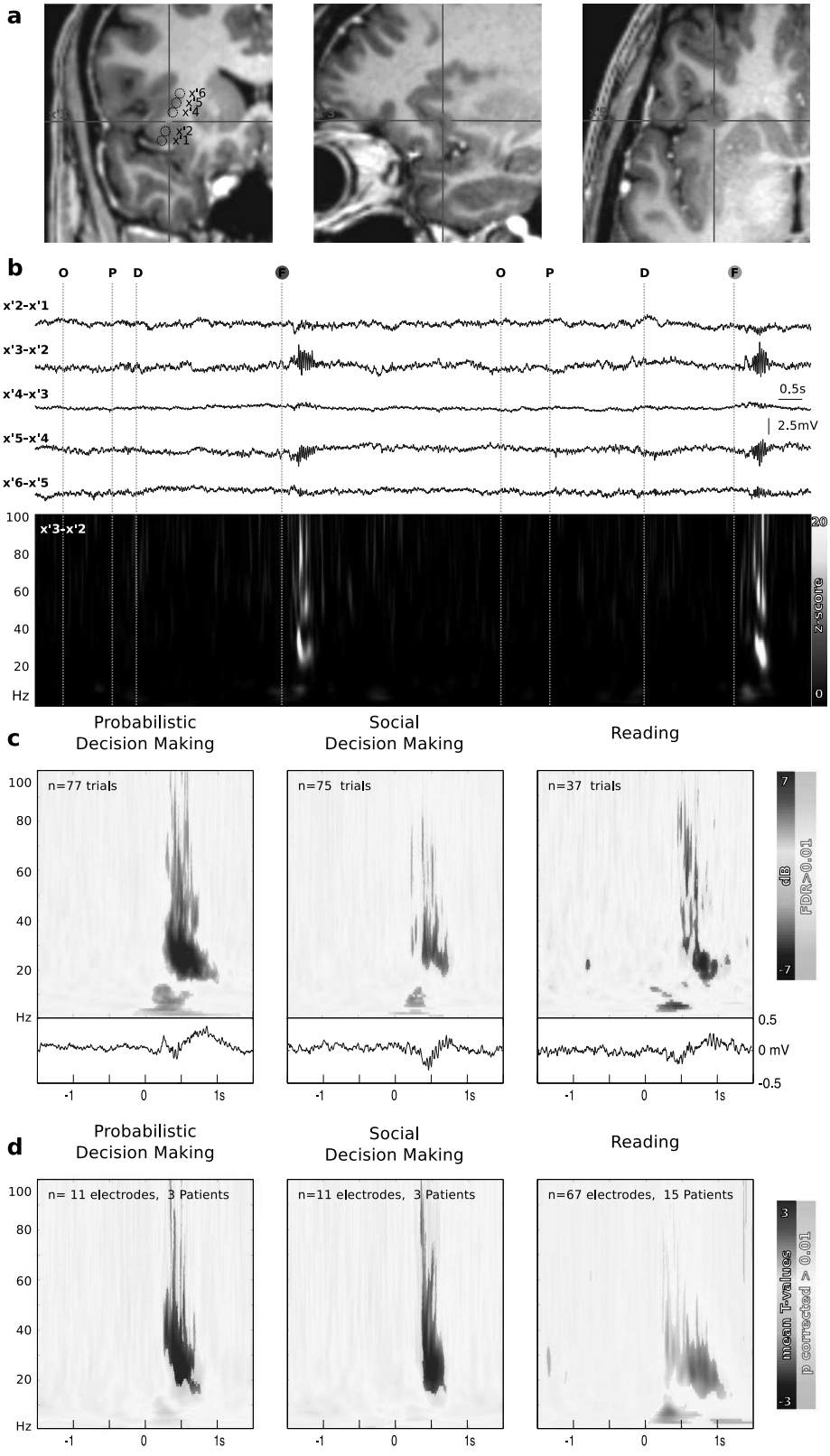

Figure 1. Neural response of the AIC to behavioral feedback during cognitive tasks. (*a*) Location of recording electrodes in the anterior insula in a subject on magnetic resonance imaging (S1). (*b*) Wideband electrical recordings (0.1–200 Hz) of the bipolar derivation of the AI electrodes and the time–frequency decomposition of $\times'3$–$\times'2$ derivation during the same period. Colors represent z-score. O: option presentation, P: presentation of the probability of each option, D: patient's decision, F: performance feedback presentation (red circle: negative feedback, green circle: positive feedback). (*c*) Time–frequency chart and event-related potential evoked by performance feedback presentation in three different tasks ($\times'3$–$\times'2$ derivation, P1). Highlighted areas represent significant modulation related to baseline (Wilcoxon test and FDR, $q < 0.01$). (*d*) Group analysis of the same three tasks. Highlighted areas represent significant modulation related to the task model (see Methods and Supplementary Fig. 8 for group analysis per all tasks).

the feedback period and the baseline using the Wilcoxon sign test. We correct for multiple comparisons using a cluster-based permutation test (Maris and Oostenveld 2007). The initial threshold for cluster detection was $P < 0.05$, and the final threshold for the significant cluster was $P < 0.01$. For the analysis of the PAC in the frequency range of interest, the LFP signal was bandpass filtered for slow-wave and beta and gamma oscillations (1–3, 15–25, and 40–100 Hz, zero phase shift noncausal finite impulse filter with 0.5-Hz roll-off). Then, the derived signal was Hilbert transformed, and the angle for the lower and the power for higher frequency band were extracted. The amplitude was then z-normalized related to a baseline period 1 s before feedback. We then performed a linear-circular correlation between the phase of lower oscillation and the amplitude of higher oscillation. Additionally, we computed a Rayleigh test. For this analysis, we compared whether the angle of the lower frequency in time points when the higher frequency has a power over 3 SD over the baseline period was nonuniform distributed in the circle. Using this approach, we computed the mean of the angles per each trial. We then compared whether these "preferred angles" were different between negative and positive feedback using a circular multisample test for equal means (circular ANOVA). The same approach was used for the PAC between the phase of the AIC beta oscillation and the power of gamma oscillation in other cortical areas.

Phase Synchrony

We calculated phase synchrony in brain signals using the phase-locking value (PLV) computed between the pairs of electrodes (Lachaux et al. 1999). The PLV measures the inter-site-phase-clustering. To compute the PLVs, we used a complex Morlet's wavelet function of seven cycles. Through this complex wavelet transform, an instantaneous phase $\phi_i^{tr}(t,f)$ is obtained for each frequency component of signals i (electrodes) at each trial (tr). The PLV between any pair of signals (i, k) is inversely related to the variability of phase differences across trials:

$$PLV_{ik}(t,f) = \frac{1}{N_{tr}}\left|\sum_{tr=1}^{N_{tr}} \exp^{j\left(\phi_i^{tr}(t,f)-\phi_k^{tr}(t,f)\right)}\right|,$$

where N_{tr} is the total number of trials. If the phase difference varies little across trials, its distribution is concentrated around a preferred value and PLV ~ 1. In contrast, under the null hypothesis of a uniformity of phase distribution, PLV values are close to zero. Finally, to assess whether two different electrodes are functionally connected, we calculated the significance probability of the PLVs by a Rayleigh test of uniformity of phase. According to this test, the significance of a PLV determined from N_{tr} can be calculated as $P = \exp^{(-N_{tr}PLV^2)}$ (Fisher 1995). To correct for multiple testing, the cluster-based permutation test (Maris and Oostenveld 2007) was applied to the time–frequency chart.

Causal Interactions

To evaluate the influence of the AI region over other feedback activated regions, we estimated Granger causality (GC) (Bressler and Seth 2011) between selected recording sites. The causality was calculated over time series across trials during performance feedback processing (0–1 s windows after feedback presentation). Each time-series was then detrended, demeaned, and first-order differencing was applied. The stationary of the processed data was tested using the autocorrelation function for each electrode. No violations of covariance stationarity were detected. Since neither the Akaike nor Bayesian information (Seth 2005) criterion yielded an optimal model order conclusively, the lowest order that led to 80% of the data to be captured by the autoregressive model was used. Then, the GC terms were computed. The significance of the difference of influence terms was determined using permutation testing (500 permutations) using two approaches. First, as in prior work (Perrone-Bertolotti et al. 2012), we permuted the signal in time windows (100 ms each), leading a measure of the significant in causal influences between the two sites. Second, pooling the trials related to feedback and control stimuli, and then selected a random group of the same number of the original feedback group. The latter approach gives us a measure of the significant influence between sites which is specific to feedback processing (that is, greater than that of control condition). The similar methods were used to calculate spectral GC (Geweke 1982). For a given spectral GC influence, we used the bootstrap method (500 bootstrap iterations) across epochs to estimate the 95% confidence intervals in order to determine whether the GC influences in both directions were significantly asymmetric. Under the null hypothesis, GC influences in both directions stem from the same distribution, and their expected difference is zero. Therefore, we observed the differences between GC influences that were tested against that the value of zero.

Software and Statistics Summary

Processing of anatomical images and electrode localization procedures were performed using the SPM8 (http://www.fil.ion.ucl.ac.uk/spm. RRID:SCR_007037) and in-house MATLAB routines (available online as LANtoolbox, http://neurocics.udd.cl, RRID:SCR_017629). Signal analysis and statistics were also implemented in LANtoolbox (Zamorano et al. 2014; Billeke et al. 2014a). For circular analysis, we used CircStat (RRID:SCR_016651). For GC, we used the MVGC multivariate GC toolbox (Seth 2010, RRID:SCR_015755). $P < 0.05$ was considered significant. We used in most cases nonparametric tests (e.g., Wilcoxon, permutation test). For all parametric tests, data were normally distributed as indicated by nonsignificance in the Kolmogorov–Smirnov test.

Results

Beta Oscillatory Activity in the AIC Reflects Performance Feedback Processing

We recorded electrical brain activity from 19 patients with intracortical electrodes located in the insular cortex. Patients were evaluated in at least two out of five cognitive tasks (see Methods), all of which included a visual cue that provided feedback on behavioral performance on each trial. For neither task, the feedback was aligned with the subject's responses. Patients carried out two decision-making tasks (PDM, Supplementary Fig. 1; and SDM, Supplementary Fig. 2), one RdT (Supplementary Fig. 3), and two working memory tasks (vWM, Supplementary Fig. 4; and sWM, Supplementary Fig. 5). In the decision-making tasks, a positive feedback represents a symbolic monetary reward outcome, while a negative feedback represents a nonreward result without a loss (no real money was given to the subject). In the remaining tasks, feedback consisted of an indication of subject performance on each individual trial (negative feedback indicated an error). The proportion of negative/positive valence

of the feedback varied by the context given by both tasks and conditions (see Supplementary Table 1). Both decision-making tasks presented greater ratio of negative valence feedback (PDM: 0.39, SDM: 0.5), whereas the other task presented less ratio of negative feedback (RDT: 0.13; vWM: 0.22; sWM: 0.07).

The presentation of the visual performance feedback evoked a prominent oscillatory response, specifically in those electrodes located in the AIC (see Fig. 1, e.g., Patient S1). This activity was absent during the presentation of most of the other relevant stimuli during all of the five behavioral tasks used. The spectral response was characterized by an early low-frequency response (1–15 Hz, Fig. 1c), followed by a burst of activity in a higher frequency range (main burst: 15–30 Hz; secondary burst: 40–100 Hz; Fig. 1c and Supplementary Figs 6–8). Group analysis from all electrodes in the AIC is shown in Fig. 1d, Supplementary Fig. 8. For our subsequent analysis, we first focused on the beta frequency range (15–30 Hz) because this oscillatory activity presented the most pronounced peak in the spectrogram (see Supplementary Figs 6 and 7 for other frequency bands).

In order to quantify the active (responsive) electrode over all the cortex, we used the activity in the feedback during RdT, which is a task that all subjects carried out to select active electrodes. We found 44 active electrodes (out of 247) in the insular cortex, where the proportion of active/inactive electrode was no different in relation to the rate of the active electrode all over the cortex (12 patients with active electrodes, rate of active electrodes in insular cortex, 0.16, all over the cortex 0.17, $P = 0.68$, permutation test). By contrast, for the electrodes located in AIC (following division proposed in Jakab et al. 2012), the proportion of active electrodes was significantly higher than both, all the cortex and the posterior insular cortex altogether (0.46, 31 electrodes out of 67, 7 patients out of 15, $P = 1e^{-5}$, permutation test, see Supplementary Fig. 7). Indeed, the posterior insular cortex presented a significantly lower rate of active electrodes in comparison with all the cortex (0.08, 13 out of 159, $P = 8e^{-5}$). The AIC seems to have a specific feedback response; hence, the subsequent analysis was focused on AIC electrodes ($n = 67$, patients = 15).

Since prior work has shown a specific role of the insula in the error processing, we then tested if the feedback processing related to AIC beta activity was different between negative and positive feedback. To this end, we studied the time course of beta oscillatory power during the processing of different task-relevant stimuli. We used the instantaneous amplitude of the signal (bandpass filtered and Hilbert transformed), and per each temporal bin, we fitted a GLM (see Methods for more details). In this model, we used two regressors, namely the performance feedback and its valence (negative or positive). Using the former regressor, we assessed whether the beta oscillatory activity was higher for feedback processing than for the processing of other salient stimuli during task performance (e.g., option presentation during the PDM task; see Methods). Additionally, using the latter regressor, we assessed for possible beta activity modulation between positive and negative feedback.

From the 31 active electrodes (7 patients out of 15) in the AIC, we found 24 electrodes (7 patients out of 15) that presented an additional modulation by feedback valence during RdT. Figure 2a shows an example of an electrode exhibiting similar responses for both negative and positive feedback, while Figure 2b shows an example for an electrode with higher responses to positive feedback in a task (represented by the blue line). In Figure 2d, we show a density map of electrodes with significant beta oscillatory responses during at least two tasks. We also found significant beta oscillatory activity in the precentral motor area, the inferior frontal gyrus (IFG), and the SMA/dACC (Fig. 2c). Additionally, we explored both gamma (40–100 Hz) and alpha (5–15 Hz) bands during feedback response. Supplementary Figure 6 shows the density map of electrodes with modulation in those frequency ranges. Although gamma and alpha responses were comparable with beta responses, the number of AIC electrodes with the beta activity was higher (Supplementary Figs 6–8). Interestingly, when comparing the valence modulation throughout different tasks, we found a variation in this response among tasks (Supplementary Figs 8 and 11).

The Amplitude of AIC Beta Oscillatory Activity Correlated with the Probability of Feedback Valence (Unsigned Prediction Error)

As we found that the valence response changed in relation to the task (Supplementary Figs 8 and 11) and that different tasks have a different ratio of negative feedback, we tested if variation in beta power encoded the probability to obtained valence feedback other than the obtained one.

For this, in each AIC electrode and across tasks, we compared both the estimated feedback response (i.e., the "feedback" regressor of the GLM which represents the beta power increase during both positive and negative feedback in comparison with other relevant stimuli during each task; see above and Methods) and the estimated feedback valence response (i.e., the "valence" regressor of the GLM which represents the beta power difference between negative and positive feedback). We found that tasks with more difficulty (i.e., greater ratio of negative feedback, e.g., during SDM and PDM tasks) were associated with more beta power on positive feedback. Conversely, a task with less difficulty (i.e., a smaller ratio of negative feedback, e.g., during vWM and sWM tasks) was associated with less beta power on negative feedback (Supplementary Figs 10 and 11).

In order to evaluate the statistical significance of this modulation, in each subject, we selected the electrode with the highest feedback response in RdT task. We correlated its estimated feedback response with the error rate (used as a proxy of task difficulty and estimated per each subject and task; see Methods). We found a statistically significant correlation for feedback responses (15 AIC electrodes [one per patient] and 5 tasks, $n = 42$, note that not all the subjects carried out all the 5 tasks, rho = 0.487, $P = 0.001$, Fig. 3). We confirmed this result using a mixed linear model (Bagiella et al. 2000) in order to rule out differences given by the intersubject variability on electrode location ($t_{40} = 3.48$, $P = 0.001$; random effect for intercept and slope, patients and tasks as grouping factor). Hence, beta oscillatory activity seemed to be larger when positive feedback valence was less probable to obtain, given the context of the difficulty of the task performed.

To evaluate whether the proceeding between-task modulation was related to a within-task modulation, we explored the trial-by-trial modulation in the power of beta oscillatory activity for each patient and each task. As a proxy of trial difficulty, we used specific task indicators of the probability of obtaining positive feedback, for instance, the amount of items to memorize for memory tasks or the explicit probability to win in PDM task. Thus, we found that, within the same task, there was a correlation between the probability of obtaining

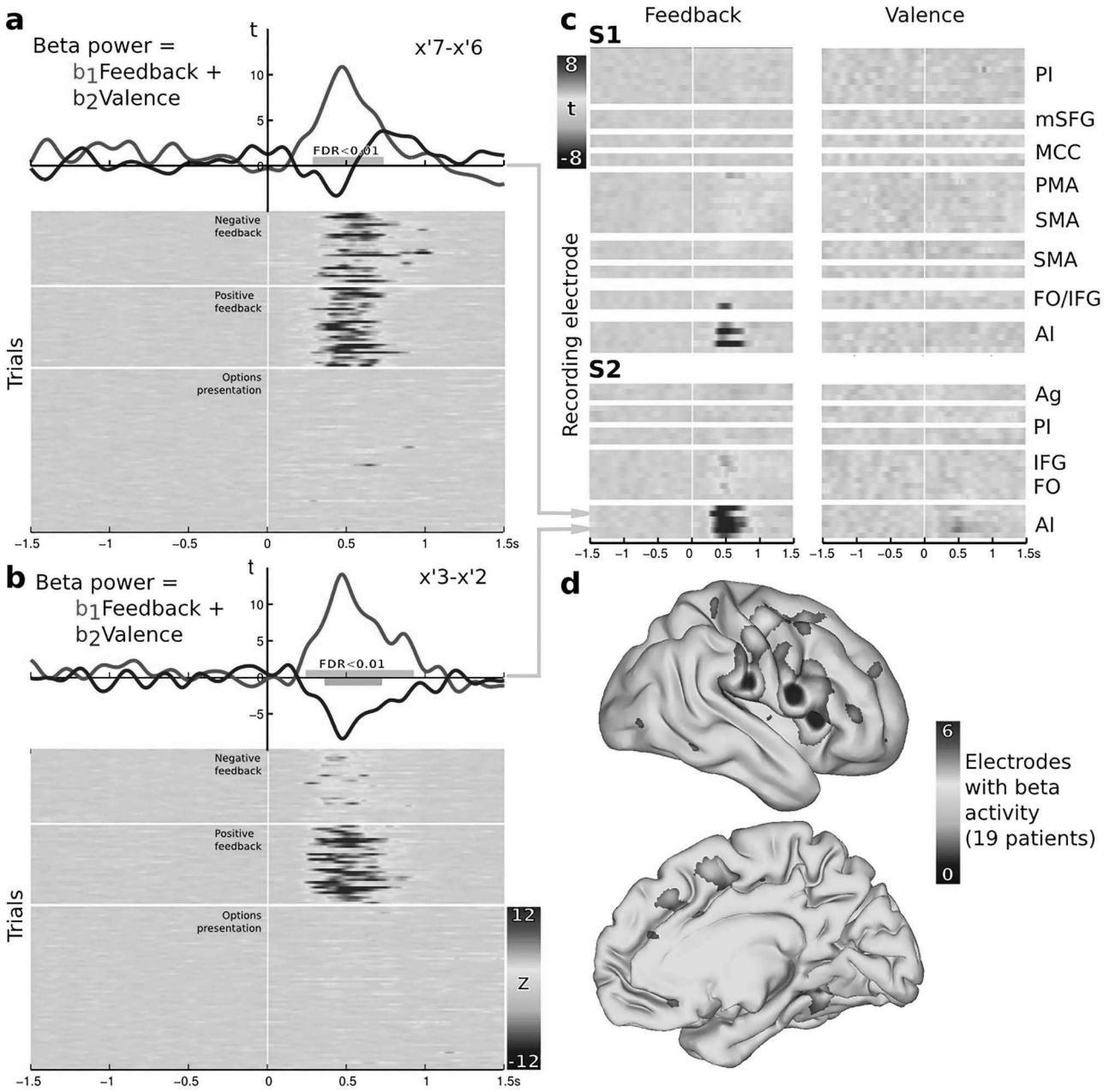

Figure 2. Beta oscillatory activity in the AIC in response to feedback presentation during the PDM task. (*a*,*b*) Single trial time-course of the amplitude of beta frequency band (15–40 Hz) related to feedback and option presentation. Color represents the power of the beta band in z-score (baseline between −1.5 and 0 s). Line plot depicts the time-course of t-values of each regressor in the model (see Methods). Red represents the feedback regressor (i.e., power response during performance feedback), and blue shows the valence regressor (i.e., the difference in power response between negative and positive feedback). Colored rectangles represent areas where regressors are significant (corrected using FDR $q < 0.01$). (*c*) Time course of t-values of regressors per electrodes in Patients S1 and S2. Note the robust response in the AIC, and the weaker activation of PMA, SMA; IFG and FO. (*d*) Density map representing the number of active electrodes in all 19 patients. Both hemispheres are pooled. See also Supplementary Figure 6. PIC: posterior insula cortex; mSFG: medial superior frontal gyrus; dACC: dorsal anterior cingulate cortex; PMA: primary motor area; SMA: supplementary motor area; FO: frontal operculum; IFG: inferior frontal gyrus; AIC: anterior insular cortex; Ag: amygdala. See also Supplementary Figs 8–11.

positive feedback and the amplitude of beta oscillatory activity (RdT: 67 electrodes, 15 patients, mean rho = −0.17, Wilcoxon test testing that rho for all electrodes was other than zero, $P = 0.0005$; see Fig. 3*b*–*e* for individual electrode examples). For negative feedback, we found the opposite pattern for both the PDM and SDM tasks (11 electrodes, 3 patients, mean rho = 0.11, $P = 0.02$; individual electrode examples: DM S1, rho = 0.38, $P = 0.02$, linear robust model, $t_{31} = 1.4$, $P = 0.16$; SDM S2, rho = 0.5, $P = 0.003$, linear robust model $t_{29} = 3.06$, $P = 0.004$). For the other tasks (RdT, sWM, and vWM), there were not enough cases of negative feedback to carry out the correlation analysis. Hence, AIC activity correlated with the probability of obtaining a result different than the obtained one. These results could indicate that beta oscillatory activity in the AIC encodes unsigned prediction error of feedback valence, which is compatible with a saliency signal.

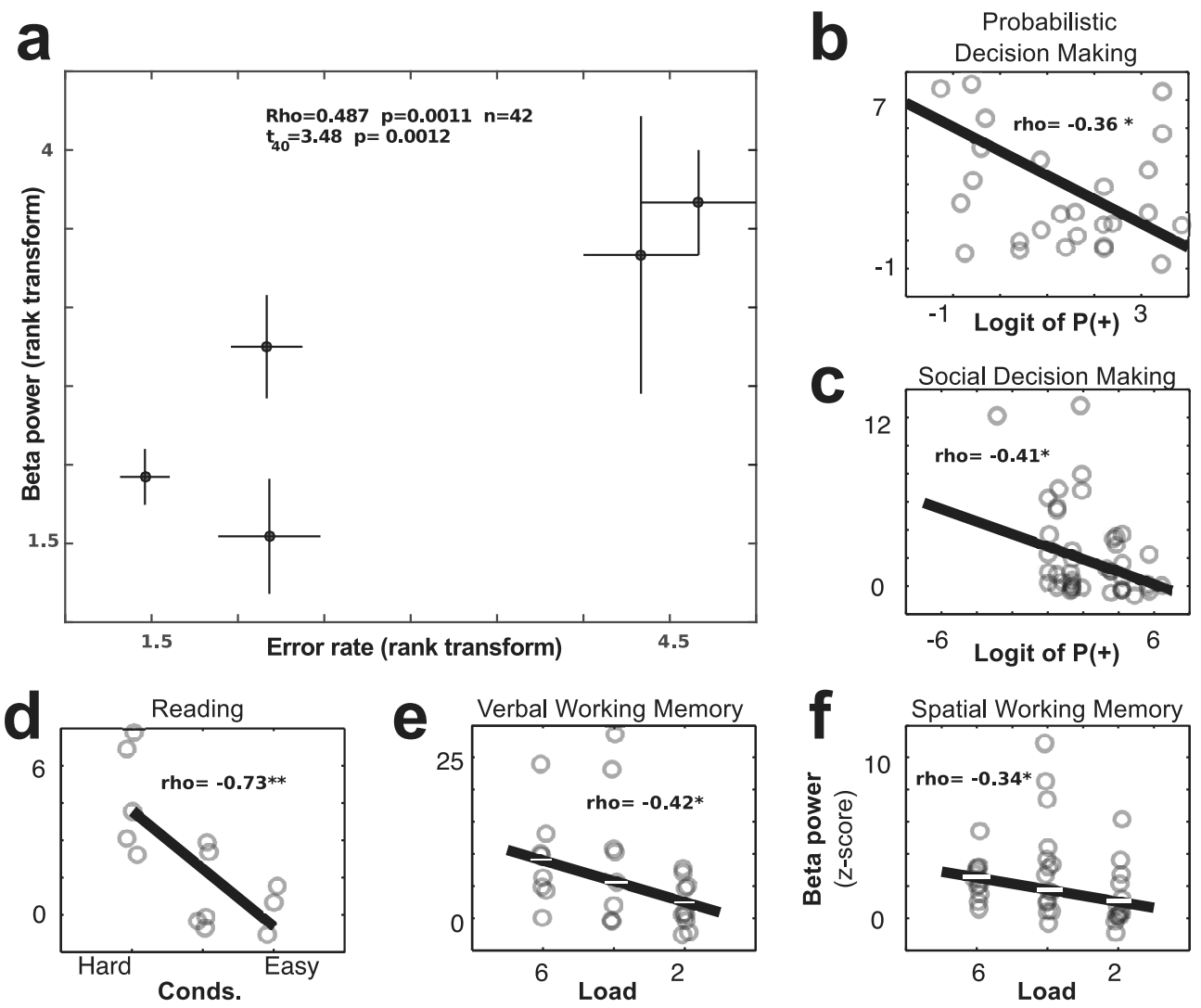

Figure 3. (*a*) Correlation between error rate (as a proxy of task difficulty) and beta oscillatory response in the AIC. For each subject ($n = 15$), we selected the electrode with the greatest response in RdT. Circles represent the mean of the rank transformed of power of beta oscillatory activity and rank transform of difficulty per task (for visualization purpose only). The line represents standard errors. (*b–f*) Individual examples of electrodes where we carried out a single trial correlation per task. (*b*,*c*) Single-trial correlations between the probability of obtaining monetary reward (logit transform) and beta oscillatory activity during positive feedback in both PDM (*b*) and SDM tasks (*c*). (*d*) Single trial correlation between difficulty of task conditions and beta oscillatory activity during positive feedback in the RdT. (*e*,*f*) Single trial correlations between memory loads and beta oscillatory activity during positive feedback in both vWM (*e*) and sWM (*f*) tasks. Lines represent robust linear regressions. Rho values were estimated using Spearman correlation. Individual examples are as follows: (*b*) PDM S1, rho = −0.36, $P = 0.02$, linear robust model $t_{30} = -2.69$, $P = 0.02$; (*c*) SDM S2, rho = −0.41, $P = 0.01$, linear robust model $T_{43} = -2.33$, $P = 0.02$; (*d*) RdT S4, rho = −0.73, $P = 0.0038$, linear robust model $T_{11} = -3.17$, $P = 0.008$; (*e*) vWM S4: rho = −0.43, $P = 0.02$, linear robust model $t_{24} = -2.1$, $P = 0.05$; (*f*) sWM S6, rho = −0.34, $P = 0.03$, linear robust model $T_{38} = -2.16$, $P = 0.03$.

Phase–Amplitude Coupling between Delta Waves and Beta Oscillatory Activity Encodes Feedback Valence

Recent studies suggest that neural activity encodes and transmits information through a structured oscillatory activity, which can be reflected in nested oscillations (Staresina et al. 2015). Thus, to explore the mechanism by which oscillatory activity encodes feedback information, we computed phase–amplitude coupling (PAC) relationships during neural processing of performance feedback. We first computed the circular-linear correlation between low-frequency (from 0.5 to 35 Hz) phases and high-frequency (from 10 to 120 Hz) powers. We next compared these correlations during feedback responses and baseline periods (0–1 s and −1 to 0 s at about the feedback presentations, respectively, in all AIC electrode during RdT, 15 patients, see Supplementary Fig. 12 for all tasks). This yielded a cluster that showed an increase in PAC (Fig. 4*a*) where delta oscillation (1–3 Hz) phase-modulated the power of beta oscillations (20–30 Hz). In order to explore the relation between this modulation an evoked responses derived from a stimulus, we correlated the cross-frequency modulation with intertrial phase coherence and power modulation in delta oscillation. We did not find a significant correlation, indicating that this modulation seems not to be given by an evoked response in delta range (absolute rho values < 0.12, P values > 0.3, canonical and partial Spearman correlations, $n = 67$ electrodes, 15 patients,

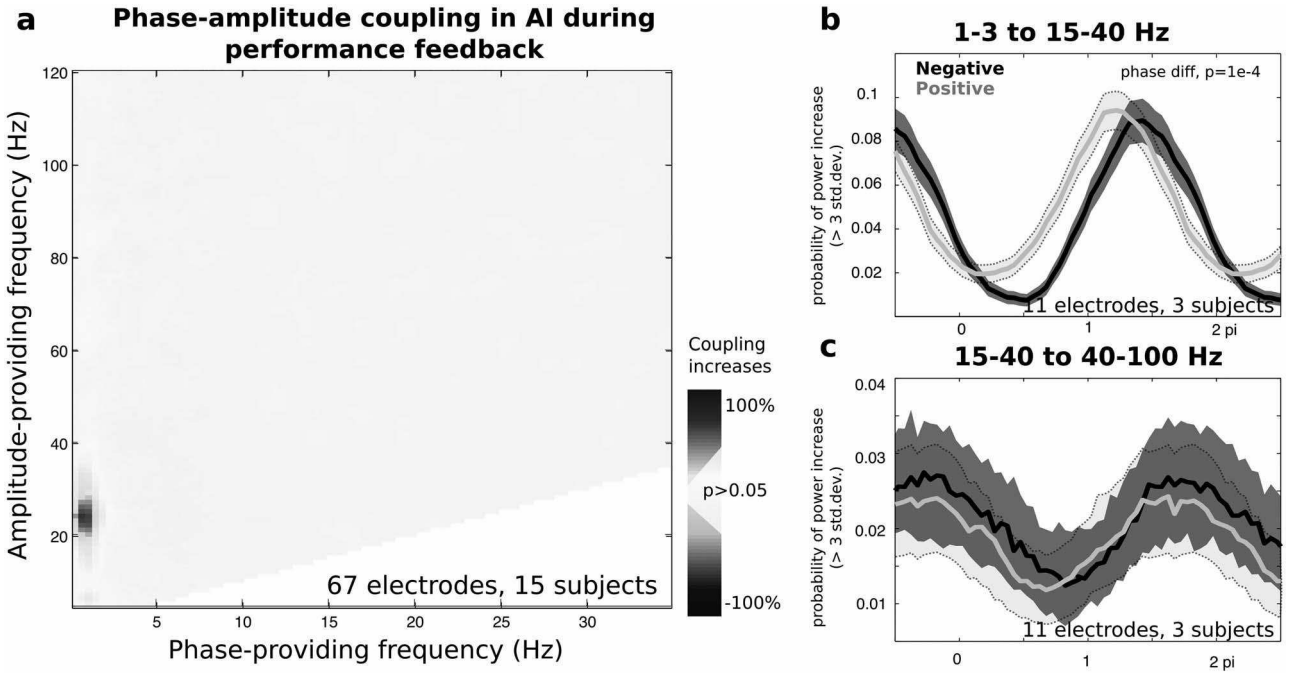

Figure 4. PAC during feedback processing in the AIC. (*a*) Color scale represents the increase in circular-linear correlation during feedback in comparison with baseline period all electrodes in the AIC (67 electrodes, 15 patients, during RdT). Statistically significant clusters are highlighted (Wilcoxon test and FDR, $q < 0.05$). (*b*,*c*). Probability of occurrence of power increments for high-frequency activity sorted by the phase of low-frequency activity during PDD and SDM task (11 electrodes, 3 patients). Feedback is separated by positive (dark) and negative (light) valence. Note significantly different phase preferences for both positive and negative feedback in delta (1–3 Hz) to beta (15–30 Hz) modulation. Shaded areas represent 95% confidence intervals. (*b*,*c*) Are individual examples of significantly modulated electrodes. See also Supplementary Figure 12.

RdT). In the task that elicited more negative feedback (PDM and SDM tasks), other clusters occurred where beta oscillation (20–35 Hz) phase-modulated the power of high gamma oscillation (80–100 Hz, Supplementary Fig. 12). This result could point to the existence of a structured oscillatory activity that may potentially encode feedback-related information. Thus, for each trial, we computed the PAC of the delta and beta oscillations. In this analysis, we used only the PDM and SDM tasks because they presented relatively balanced amounts of negative and positive feedback cases (a mean of 43.4% negative feedback). For each of the 11 electrodes analyzed (three patients), we found significant modulations ($P < 0.05$, Rayleigh test and circular-linear correlation). When comparing negative and positive feedback, the preferred phases differed by a mean of 39.8° (the difference was significant in 8 out of the 11 electrodes, $P < 0.05$, circular multisample test for equal means, one-factor ANOVA; Fig. 4*b*). Since broadband, rather than narrowband, modulation has been correlated with local neuronal population spiking rates (Manning et al. 2009), we next explored whether the phase of beta oscillations modulated the amplitude of broadband gamma activity (60–120 Hz). In fact, we found significant modulation in 10 out of the 11 electrodes ($P < 0.05$, Rayleigh test and circular-linear correlation). We did not find consistent differences between positive and negative feedback for the preferred phases of this PAC. These results suggest that the AIC encodes feedback information throughout structured cross-frequency coupling among delta, beta, and gamma oscillations. Moreover, specific feedback valence information is encoded via the preferred phase of the delta-beta PAC.

Beta Oscillatory Activity in AI Modulates mPFC

Since the synchronization of beta oscillations has been recently associated with feedback projection in top-down processes (Buschman and Miller 2007; Pesaran et al. 2008; Wang 2010; Buschman et al. 2012; Bastos et al. 2014), we explored phase synchrony between the AIC and cortical areas in the medial prefrontal region. For this, we explored connectivity between the AIC electrode with the highest response per subjects (during RdT) and any electrodes located in the medial prefrontal region (see method for electrode localization, 19 pairs of electrodes, 4 patients, see Fig. 2*d* and Supplementary Figs 7, 9 and 13). We first computed phase synchrony (i.e., inter-site-phase-clustering, phase locking value) and found a beta-band synchronization after feedback presentation (Fig. 5*a*). Synchronization in the beta band can potentially exert its influence by changing the firing rate and broadband gamma power in target cortices (Wang 2010). We thus explored whether the phase of beta oscillations in the AIC modulated the gamma power of target cortical regions. We found that the phase of AIC beta oscillations significantly modulated the power of the gamma band activity (0–1 s after feedback presentation, Fig. 5*b*). These results provide evidence for a putative mechanism used by AIC to modulate the activity of frontal regions.

In order to establish a causal influence of the AIC on mPFC, we computed the GC (in both time and frequency domains) between the AIC and the frontal regions that exhibit feedback response (0–1 s after the feedback presentation). We also tested whether these influences during feedback processing were highest than those during the processing of other relevant

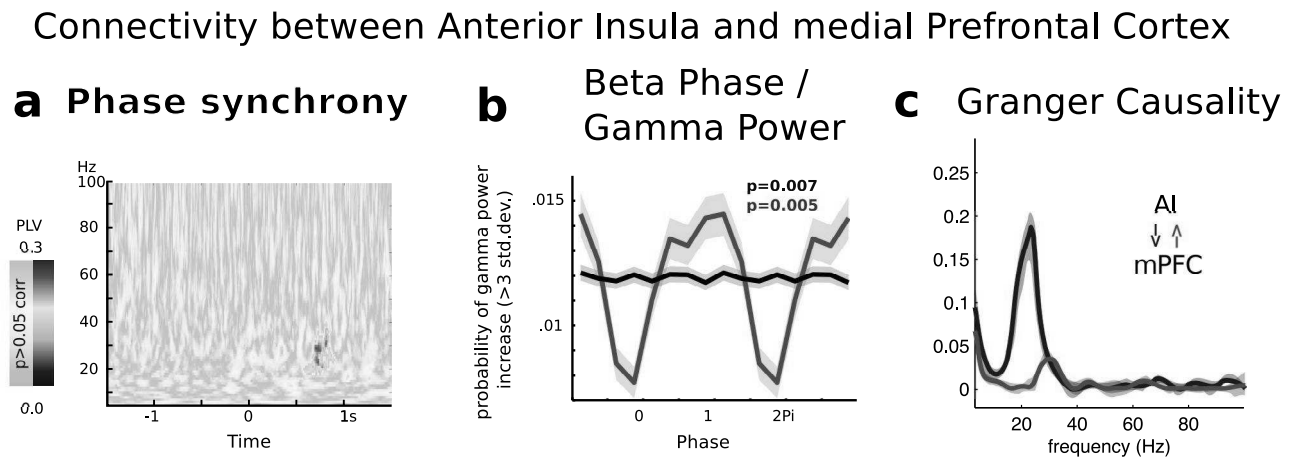

Figure 5. Functional connectivity between the AIC and medial prefrontal areas. (*a*) Inter-site-phase-clustering. Color scale represents the PLV. Statistically significant clusters are highlighted (cluster-based permutation test). (*b*) The phase of the beta frequency band (15–30 Hz) in the AIC modulates the power of gamma band (40–100 Hz). Red lines represent the probability of gamma power increase over 3 SD in comparison with the baseline. Black lines represent the permutation distribution (see Methods). *P*-values were computed using both the Rayleigh test (top) and circular-linear correlation (down). (*c*) Frequency domain of the Granger causal influence. See also Supplementary Figure 10. Shaded areas represent 95% confidence intervals. For all figure, 19 pairs of electrodes, four patients, during RdT.

Table 1 Single trial correlation of Granger causal influence (AI → ACC) in beta range (15–30 Hz) during PDM task ($n = 84$ trials, Patient S1)

	Slope	SE	*t*	*P*
Intercept	0.267	0.063	4.219	0.0001
Feedback valence (positive)	−0.01	0.14	−0.07	0.9446
Probability (logit)	−0.08	0.029	−2.784	0.0067
Interaction F × P	0.1223	0.06	2.052	0.3323
Payoff	−0.249	0.229	−1.09	0.28

stimuli (see Methods). The most consistent influence was a causal interaction of the AIC to medial frontal cortices (four out of four patients, $P \leq 0.02$). In Supplementary Figure 11, we detail the location of all electrodes in the medial frontal region, where the AIC causally influenced oscillatory activity. Causal influences were mainly generated by beta oscillations (15–30 Hz, Fig. 5c, and Supplementary Fig. 13). Finally, we focused on the PDM task, since payoffs and the probability of the feedback were independent. Using single-trial variations in the Granger causal influence, we explored the information transmitted from the AIC to the dACC during feedback processing. The variation in the Granger influence in the beta range mainly correlated with the probability of feedback valence and did not correlate with either payoffs or valence per se (Table 1 and Supplementary Fig. 14). Our results suggest that AIC beta activity causally influences medial prefrontal regions, transmitting specifically an unsigned prediction error signals.

Discussion

Our results provide evidence for a role of and suggest a mechanism by mean the AIC process both the valence and the probability of performance feedback valence. During feedback signaling consequences of a decision, the AIC is engaged in structured oscillatory activity. The structure of this oscillatory activity seems to be related to the encoding/transitions of different properties of performance feedback. In particular, the PAC between delta and beta oscillations reflects the valence of the feedback, while the beta oscillations reflect the coding and transition of the probability of performance feedback valence (the probability to obtain a feedback valence other than the obtained one, i.e., unsigned prediction error) to other cortical areas.

The AIC has been observed to be involved in high-level cognitive processes, such as task switching, inhibition, and error processing (Uddin 2014; Bastin et al. 2016). Previous work shows that the AIC presents more activity in relation to negative feedback or error, than to positive feedback (Dosenbach et al. 2006; Ham et al. 2013; Neta et al. 2014; Bastin et al. 2016). Indeed, evidence from fMRI studies shows stronger AIC activity when an error takes place than that generated when a salient infrequent stimulus is detected (Wessel et al. 2012). Based on such evidence, it has been proposed that the AIC has a role in error awareness (Klein et al. 2013). In contrast, we found that beta oscillatory activity in the AIC was associated with both positive and negative performance feedback. In low-difficulty tasks, robust beta oscillatory activity was associated with errors, or negative feedback. In contrast, in high-difficulty tasks (i.e. error rate > 30%), beta oscillatory activity was larger for positive feedback than for negative feedback.

Interestingly, a recent across-task study (Neta et al. 2015) shows that performance feedback processing activates a brain network, which includes several of the cortical areas we described in the analysis of all our patients (Fig. 2*d*). Contrary to our results, the study did not find a significant effect of accuracy in insular cortex activation. This discrepancy may be due to the fact that most studies typically use tasks with low error rates (<25%; Dosenbach et al. 2006; Neta et al. 2015). Importantly, the beta amplitude modulation that we found across tasks also occurred trial-by-trial within the same task. That is, positive feedback under challenging trials generated stronger beta activity than that generated in easy trials during the same task. Thus, our findings are in agreement with the notion of an unsigned prediction error or saliency signal. In other words, the AIC seems to signal the probability of obtaining a feedback valence other than the obtained one, irrespective of its specific nature (positive or negative). Thus, a possible interpretation is that subjects generate an internal signal of

the expected feedback valency, which is contrasted with the obtained feedback. Thus, the beta oscillatory modulation can reflect the unexpectedness of feedback valence. This property, which has often been generically referred to as salience, provides support for the view that the AIC is involved in learning. For instance, BOLD signals reported in AIC have been shown to be related to both aversive and appetitive learning (Seymour et al. 2005). Indeed, recent fMRI studies showed that the activity in AIC is part of a brain network that governs an adaptive learning rate (McGuire et al. 2014; Jiang et al. 2015). These studies proposed that AI/IFG encodes the need to change/adapt the learning rate related to changes in the uncertainty of the environment. Interestingly, AIC BOLD activity has shown to correlate with medial prefrontal activations, in the region where we found significant causal influence from AIC. These medial frontal regions are thought to be related to the implementation of subsequent cognitive control (Shenhav et al. 2013). Thus, the role of the mPFC, as an action-outcome predictor (Alexander and Brown 2011), may depend crucially on the information provided by the AIC. Taken together, we propose that the AIC encodes to which extent the information of performance feedback entails the need to adapt both the expectations related to future stimulus but also the behavioral strategy. This interpretation is consistent with several fMRI studies that showed robust AIC activity related to cues indicative of changes in either strategy or difficulty (Dosenbach et al. 2006, 2007).

In addition to the documented role of beta oscillations in motor control and organization of neuronal assemblies (Engel and Fries 2010), recent evidence indicates that the synchronization of the prefrontal cortex in beta frequency range has a role in both strategy switching and selection (Buschman et al. 2012), as well as in the maintenance of cognitive control over time (Bastin et al. 2014; Stoll et al. 2015). Several EEG studies have shown that performance feedback, or reward delivery, generates beta oscillatory activity, which can be detected in medial prefrontal scalp electrodes (Marco-Pallares et al. 2008; Billeke et al. 2013, 2015). This activity correlates with the BOLD signal in both the mPFC and the IFG (Mas-Herrero et al. 2015). Interestingly, we found that the amplitude of beta oscillatory activity in the AIC encodes the probability of feedback valence and relays this information to the mPFC. This could, in turn, implement adaptive behavioral changes (McGuire et al. 2014). Moreover, the intrinsic structure of AIC oscillatory activity, reflected in its hierarchically organized nested frequencies, encodes other features of feedback. In fact, we found that the amplitude of beta oscillations was modulated by the phase of delta waves and that, according to feedback valence (positive or negative), the preferred phase for this modulation was distinctive. Prior work has suggested that cross-frequency coupling is a mechanism through which neuronal assemblies organize and relay information (Lisman and Jensen 2013; Jensen et al. 2014; Billeke et al. 2017; Figueroa-Vargas et al. 2019). Indeed, in other studies of cortical recordings in humans, it can be observed that the phase of low frequency organizes the modulation of high-frequency oscillation amplitude depending on the kind of visual information processed (Watrous et al. 2015). Additionally, in prefrontal regions, the PAC between theta and gamma oscillations is thought to reflect information transmission about task demands (Voytek et al. 2015) and information to maintain in working memory (Roux and Uhlhaas 2013). The strength of PAC between delta and gamma-band activities in the fronto-parietal network has been related to performance during an attentional task (Szczepanski et al. 2014). Thus, the organization of oscillatory activity throughnested frequencies seems to be a general mechanism by which complex information is processed and transmitted across the cortex (Staresina et al. 2015; Billeke et al. 2017; Figueroa-Vargas et al. 2019).

Currently, it has been proposed that both beta and gamma activity can be better understood as a burst-like activity rather than a sustained oscillatory activity (van Ede et al. 2018). Although a temporal threshold to separate both activities is not possible, the inspection of a single trial event (Figs 1*b* and 2*a*,*b*) reveals that each event is sustained by at least 8–10 beta-cycles (~500 ms). Despite that, our analysis was not able to clearly determine the burst or sustained nature of the AIC beta activity. For the PAC analysis, we used two approaches, one better designed for a sustained activity (circular correlation, Fig. 4*a*) and the other better designed to analyze burst-like activity (thresholding analysis, Fig. 4*b*). Interestingly, both analyses are consistent in revealing that delta-beta relation is independent of the exact nature of the beta activity. Beyond this discussion, during top-down modulation of cognitive processing, slow oscillations (<30 Hz) seem to represent output projections (Buschman and Miller 2007; Pesaran et al. 2008; Wang 2010; Buschman et al. 2012; Bastos et al. 2014). Thus, theta to beta oscillations can serve as a mechanism for interregional interaction and top-down influence (Donner and Siegel 2011; Richter et al. 2017). Accordingly, our results indicate that beta oscillatory activity in the AIC reflects the coordinated operation of a phase-synchronized network, which involves several cortical regions, including the IFG, the OFC, and the mPFC (comprising the dACC). Moreover, our causal analysis showed that the AIC relays performance feedback-related information to the mPFC. Such information flow is inversely proportional to the expectancy of feedback valence, regardless of the specific feedback valence or the feedback-associated reward. In addition to the PAC between delta and beta oscillations, we found that the phase of beta oscillations modulated the amplitude of gamma-band activity. Previous reports indicate that broadband gamma modulation is correlated with spiking rates in local neuronal populations (Manning et al. 2009). Accordingly, we found that the phase of beta oscillations modulates local broadband gamma activity, likely reflecting the coordination of endogenous neural spiking in AIC.

Moreover, the phase of beta oscillations in the AIC modulated the power of broadband gamma waves in other cortical areas, possibly suggesting that beta synchronization can organize neural spiking activity in distant cortical areas. Thus, AIC beta influence over the medial prefrontal region may organize broadband gamma activity in the target region in a direct way or through beta phase–phase coupling between the two areas that modulate beta activity and, in turn, modulates local gamma power. Interestingly, recent evidence in macaques shows that top-down beta activity, in fact, modulates gamma forward information flux in visual areas (Richter et al. 2017). Hence, we propose that the AIC generates and transmits the probability of feedback valence (or unsigned prediction error) information to the mPFC through synchronization in the beta frequency band. Thus, our results suggest that locally generated beta oscillations coordinate broadband gamma activity—and putatively spiking activity—in target cortical areas. As a target region, the mPFC may integrate the information relayed by the AIC and is likely to combine it with the input from other cortical areas in order to allocate cognitive resources to produce subsequent adaptive behaviors. In spite of the greater signal-to-noise ratio of intracortical recording, it is important to point out some of the limitations of our research. The relatively small number of

paired electrodes of some of the analysis requires the replication of these results with a broader sample and different experimental techniques. Although we did not analyze any site with possible epileptic activity, it is not possible to rule out some of the disorder effects in the results.

In summary, our results provide novel insight for a rhythmic electrophysiological mechanism by which the AIC participates in the neural processing of performance feedback. Through a structured oscillatory activity, the AIC encodes the valence and probability of feedback valence. In particular, through the generation of a phase-synchronized network in the beta frequency range, the AIC transmits unsigned error prediction signals to medial prefrontal areas, which likely implement cognitive feedback control in order to learn and adjust subsequent behavior. Our results pinpoint an efficient dynamic neural mechanism for performance monitoring and adaptive behavior that carries the potential to explain the abundant evidence relating insular lesions, or insular-related neurological disorders, with disruptions in decision-making, learning, and behavioral adjustment (Kishida et al. 2010; Uddin et al. 2010; Billeke and Aboitiz 2013; Billeke 2016).

Supplementary Material

Supplementary material is available at *Cerebral Cortex* online.

Author Contributions

P.B. and J.P.L. designed the experiment; P.B. programmed the experiment; P.B., M.P.-B., and P.K. conducted the experiments; P.K. subject evaluations; P.B. analyzed the data; T.O., J.B., M.P.-B., K.J., and P.F. interpretation and discussion; P.B., T.O., K.J., J.B., and P.F. wrote the manuscript.

Funding

CONICYT, FONDECYT (1181295 and 1190513 to P.B., 1180932 and 1190375 to P.F., 1140996 to T.O., 11140535, ECOS/CONICYT C15S01, ECOS/CONICYT C12S03, CONICYT ACT1414). Canada Research Chairs program and a Discovery Grant (RGPIN-2015-04854) from NSERC (Canada), New Investigators Award from FQNT (2018-NC-206005), IVADO-Apogée fundamental research project gran, the FRQNT Strategic Clusters Program (2020-RS4-265502 – Centre UNIQUE – Union Neurosciences & Artificial Intelligence – Quebec).

Conflict of Interest

The authors report no biomedical financial interest nor potential conflicts of interest.

References

Alexander WH, Brown JW. 2011. Medial prefrontal cortex as an action-outcome predictor. *Nat Neurosci*. 14:1338–1344.

Bagiella E, Sloan RP, Heitjan DF. 2000. Mixed-effects models in psychophysiology. *Psychophysiology*. 37:13–20.

Bastin J, Deman P, David O, Gueguen M, Benis D, Minotti L, Hoffman D, Combrisson E, Kujala J, Perrone-Bertolotti M, *et al*. 2016. Direct recordings from human anterior insula reveal its leading role within the error-monitoring network. *Cereb Cortex*. 27:1545–1557.

Bastin J, Polosan M, Benis D, Goetz L, Bhattacharjee M, Piallat B, Krainik A, Bougerol T, Chabardès S, David O. 2014. Inhibitory control and error monitoring by human subthalamic neurons. *Transl Psychiatry*. 4:e439.

Bastos AM, Vezoli J, Bosman CA, Schoffelen J-M, Oostenveld R, Dowdall JR, De Weerd P, Kennedy H, Fries P. 2014. Visual areas exert feedforward and feedback influences through distinct frequency channels. *Neuron*. 85:390–401.

Billeke P. 2016. The more I get to know you, the more I distrust you? Non-linear relationship between social skills and social behavior. *Front Psych*. 7:49.

Billeke P, Aboitiz F. 2013. Social cognition in schizophrenia: from social stimuli processing to social engagement. *Front Psych*. 4:1–12.

Billeke P, Armijo A, Castillo D, López T, Zamorano F, Cosmelli D, Aboitiz F. 2015. Paradoxical expectation: oscillatory brain activity reveals social interaction impairment in schizophrenia. *Biol Psychiatry*. 78:421–431.

Billeke P, Ossandon T, Stockle M, Perrone-Bertolotti M, Kahane P, Lachaux J-P, Fuentealba P. 2017. Brain state-dependent recruitment of high-frequency oscillations in the human hippocampus. *Cortex*. 94:87–99.

Billeke P, Zamorano F, Chavez M, Cosmelli D, Aboitiz F. 2014a. Functional network dynamics in alpha band correlate with social bargaining. *PLoS One*. 9:e109829.

Billeke P, Zamorano F, Cosmelli D, Aboitiz F. 2013. Oscillatory brain activity correlates with risk perception and predicts social decisions. *Cereb Cortex*. 23:2872–2883.

Billeke P, Zamorano F, López T, Rodriguez C, Cosmelli D, Aboitiz F. 2014b. Someone has to give in: theta oscillations correlate with adaptive behavior in social bargaining. *Soc Cogn Affect Neurosci*. 9:2041–2048.

Bonini F, Burle B, Liégeois-Chauvel C, Régis J, Chauvel P, Vidal F. 2014. Action monitoring and medial frontal cortex: leading role of supplementary motor area. *Science*. 343:888–891.

Bressler SL, Seth AK. 2011. Wiener-granger causality: a well established methodology. *NeuroImage*. 58:323–329.

Buschman T, Miller E. 2007. Top-down versus bottom-up control of attention in the prefrontal and posterior parietal cortices. *Science*. 315:1860–1862.

Buschman TJ, Denovellis EL, Diogo C, Bullock D, Miller EK. 2012. Synchronous oscillatory neural ensembles for rules in the prefrontal cortex. *Neuron*. 76:838–846.

Craig ADB. 2009. How do you feel–now? The anterior insula and human awareness. *Nat Rev Neurosci*. 10:59–70.

Donner TH, Siegel M. 2011. A framework for local cortical oscillation patterns. *Trends Cogn Sci*. 15:191–199.

Dosenbach NUF, Fair DA, Miezin FM, Cohen AL, Wenger KK, Dosenbach R A T, Fox MD, Snyder AZ, Vincent JL, Raichle ME, *et al*. 2007. Distinct brain networks for adaptive and stable task control in humans. *Proc Natl Acad Sci U S A*. 104:11073–11078.

Dosenbach NUF, Visscher KM, Palmer ED, Miezin FM, Wenger KK, Kang HC, Burgund ED, Grimes AL, Schlaggar BL, Petersen SE. 2006. A core system for the implementation of task sets. *Neuron*. 50:799–812.

Engel AK, Fries P. 2010. Beta-band oscillations-signalling the status quo? *Curr Opin Neurobiol*. 20:156–165.

Ferdinand NK, Opitz B. 2014. Different aspects of performance feedback engage different brain areas: disentangling valence and expectancy in feedback processing. *Sci Rep*. 4:5986.

Figueroa-Vargas A, Cárcamo C, Henríquez-Ch R, Zamorano F, Ciampi E, Uribe R, Vásquez M, Aboitiz B, Billeke P. 2019.

Loss of interplay: frontoparietal dynamics underlie working memory deficits in multiple sclerosis. bioRxiv. 639930:1–38. doi: 10.1101/639930.

Fisher N. 1995. *Statistical analysis of circular data*. Cambridge University Press, Cambridge, England.

Geweke J. 1982. Measurement of linear dependence and feedback between multiple time series. *J Am Stat Assoc*. 77:304–313.

Glimcher PW. 2011. Understanding dopamine and reinforcement learning: the dopamine reward prediction error hypothesis. *Proc Natl Acad Sci USA*. 108:15647–15654.

Ham T, Leff A, de Boissezon X, Joffe A, Sharp DJ. 2013. Cognitive control and the salience network: an investigation of error processing and effective connectivity. *J Neurosci*. 33:7091–7098.

Hamamé CM, Vidal JR, Ossandón T, Jerbi K, Dalal SS, Minotti L, Bertrand O, Kahane P, Lachaux JP. 2012. Reading the mind's eye: online detection of visuo-spatial working memory and visual imagery in the inferior temporal lobe. *NeuroImage*. 59:872–879.

Higo T, Mars RB, Boorman ED, Buch ER, Rushworth MFS. 2011. Distributed and causal influence of frontal operculum in task control. *Proc Natl Acad Sci USA*. 108:4230–4235.

Jakab A, Molnár PP, Bogner P, Béres M, Berényi EL. 2012. Connectivity-based parcellation reveals interhemispheric differences in the insula. *Brain Topogr*. 25:264–271.

Jensen O, Gips B, Bergmann TO, Bonnefond M. 2014. Temporal coding organized by coupled alpha and gamma oscillations prioritize visual processing. *Trends Neurosci*. 37:357–369.

Jerbi K, Ossandón T, Hamamé C, Senova S, Dalal SS, Jung J, Minotti L, Bertrand O, Berthoz A, Kahane P, *et al*. 2009. Task-related gamma-band dynamics from an intracerebral perspective: review and implications for surface EEG and MEG. *Hum Brain Mapp*. 30:1758–1771.

Jiang J, Beck J, Heller K, Egner T. 2015. An insula-frontostriatal network mediates flexible cognitive control by adaptively predicting changing control demands. *Nat Commun*. 6: 8165.

Jung J, Bayle D, Jerbi K, Vidal JR, Hénaff M-A, Ossandon T, Bertrand O, Mauguière F, Lachaux J-P. 2011. Intracerebral γ modulations reveal interaction between emotional processing and action outcome evaluation in the human orbitofrontal cortex. *Int J Psychophysiol*. 79:64–72.

Jung J, Jerbi K, Ossandon T, Ryvlin P, Isnard J, Bertrand O, Guénot M, Mauguière F, Lachaux JP. 2010. Brain responses to success and failure: direct recordings from human cerebral cortex. *Hum Brain Mapp*. 31:1217–1232.

Kishida KT, King-Casas B, Montague PR. 2010. Neuroeconomic approaches to mental disorders. *Neuron*. 67:543–554.

Klein TA, Endrass T, Kathmann N, Neumann J, von Cramon DY, Ullsperger M. 2007. Neural correlates of error awareness. *NeuroImage*. 34:1774–1781.

Klein TA, Ullsperger M, Danielmeier C. 2013. Error awareness and the insula: links to neurological and psychiatric diseases. *Front Hum Neurosci*. 7:14.

Lachaux JP, Rodriguez E, Martinerie J, Varela FJ. 1999. Measuring phase synchrony in brain signals. *Hum Brain Mapp*. 8:194–208.

Lisman JE, Jensen O. 2013. The theta-gamma neural code. *Neuron*. 77:1002–1016.

Manning JR, Jacobs J, Fried I, Kahana MJ. 2009. Broadband shifts in local field potential power spectra are correlated with single-neuron spiking in humans. *J Neurosci*. 29:13613–13620.

Marco-Pallares J, Cucurell D, Cunillera T, García R, Andrés-Pueyo A, Münte TF, Rodríguez-Fornells A. 2008. Human oscillatory activity associated to reward processing in a gambling task. *Neuropsychologia*. 46:241–248.

Maris E, Oostenveld R. 2007. Nonparametric statistical testing of EEG- and MEG-data. *J Neurosci Methods*. 164:177–190.

Mark Williams S, Goldman-Rakic PS. 1998. Widespread origin of the primate mesofrontal dopamine system. *Cereb Cortex*. 8:321–345.

Mas-Herrero E, Ripollés P, HajiHosseini A, Rodríguez-Fornells A, Marco-Pallarés J. 2015. Beta oscillations and reward processing: coupling oscillatory activity and hemodynamic responses. *NeuroImage*. 119:13–19.

McGuire JT, Nassar MR, Gold JI, Kable JW. 2014. Functionally dissociable influences on learning rate in a dynamic environment. *Neuron*. 84:870–881.

Medford N, Critchley HD. 2010. Conjoint activity of anterior insular and anterior cingulate cortex: awareness and response. *Brain Struct Funct*. 214:535–549.

Melloni M, Billeke P, Baez S, Hesse E, de la Fuente L, Forno G, Birba A, García-Cordero I, Serrano C, Plastino A, *et al*. 2016. Your perspective and my benefit: multiple lesion models of self-other integration strategies during social bargaining. *Brain*. 139:3022–3040.

Menon V, Uddin LQ. 2010. Saliency, switching, attention and control: a network model of insula function. *Brain Struct Funct*. 214:655–667.

Nelson SM, Dosenbach NUF, Cohen AL, Wheeler ME, Schlaggar BL, Petersen SE. 2010. Role of the anterior insula in task-level control and focal attention. *Brain Struct Funct*. 214:669–680.

Neta M, Miezin FM, Nelson SM, Dubis JW, Dosenbach NUF, Schlaggar BL, Petersen SE. 2015. Spatial and temporal characteristics of error-related activity in the human brain. *J Neurosci*. 35:253–266.

Neta M, Schlaggar BL, Petersen SE. 2014. Separable responses to error, ambiguity, and reaction time in cingulo-opercular task control regions. *NeuroImage*. 99:59–68.

Perrone-Bertolotti M, Kujala J, Vidal JR, Hamame CM, Ossandon T, Bertrand O, Minotti L, Kahane P, Jerbi K, Lachaux J-P. 2012. How silent is silent reading? Intracerebral evidence for top-down activation of temporal voice areas during reading. *J Neurosci*. 32:17554–17562.

Pesaran B, Nelson MJ, R a A. 2008. Free choice activates a decision circuit between frontal and parietal cortex. *Nature*. 453:406–409.

Power JDD, Cohen ALL, Nelson SMM, Wig GSS, Barnes KAA, Church JAA, Vogel ACC, Laumann TOO, Miezin FMM, Schlaggar BLL, *et al*. 2011. Functional network organization of the human brain. *Neuron*. 72:665–678.

Richter CG, Thompson WH, Bosman CA, Fries P. 2017. Top-down beta enhances bottom-up gamma. *J Neurosci*. 37:3771–3716.

Roux F, Uhlhaas PJ. 2013. Working memory and neural oscillations: alpha-gamma versus theta-gamma codes for distinct WM information? *Trends Cogn Sci*. 18:16–25.

Seeley WW, Menon V, Schatzberg AF, Keller J, Glover GH, Kenna H, Reiss AL, Greicius MD. 2007. Dissociable intrinsic connectivity networks for salience processing and executive control. *J Neurosci*. 27:2349–2356.

Seth AK. 2005. Causal connectivity of evolved neural networks during behavior. *Network*. 16:35–54.

Seth AK. 2010. A MATLAB toolbox for granger causal connectivity analysis. *J Neurosci Methods*. 186:262–273.

Seymour B, O'Doherty JP, Koltzenburg M, Wiech K, Frackowiak R, Friston K, Dolan R. 2005. Opponent appetitive-aversive neural processes underlie predictive learning of pain relief. *Nat Neurosci*. 8:1234–1240.

Shenhav A, Botvinick MM, Cohen JD. 2013. The expected value of control: an integrative theory of anterior cingulate cortex function. *Neuron*. 79:217–240.

Shenhav A, Straccia MA, Cohen JD, Botvinick MM. 2014. Anterior cingulate engagement in a foraging context reflects choice difficulty, not foraging value. *Nat Neurosci*. 17:1249–1254.

Sridharan D, Levitin DJ, Menon V. 2008. A critical role for the right fronto-insular cortex in switching between central-executive and default-mode networks. *Proc Natl Acad Sci USA*. 105:12569–12574.

Staresina BP, Bergmann TO, Bonnefond M, van der Meij R, Jensen O, Deuker L, Elger CE, Axmacher N, Fell J. 2015. Hierarchical nesting of slow oscillations, spindles and ripples in the human hippocampus during sleep. *Nat Neurosci*. 18:1679–1686.

Stoll FM, Wilson CRE, Faraut MCM, Vezoli J, Knoblauch K, Procyk E. 2015. The effects of cognitive control and time on frontal Beta oscillations. *Cereb Cortex*. 26:1715–1732.

Szczepanski SM, Crone NE, Kuperman RA, Auguste KI, Parvizi J, Knight RT. 2014. Dynamic changes in phase-amplitude coupling facilitate spatial attention control in Fronto-parietal cortex. *PLoS Biol*. 12:e1001936.

Uddin LQ. 2014. Salience processing and insular cortical function and dysfunction. *Nat Rev Neurosci*. 16:55–61.

Uddin LQ, Supekar K, Amin H, Rykhlevskaia E, Nguyen DA, Greicius MD, Menon V. 2010. Dissociable connectivity within human angular gyrus and intraparietal sulcus: evidence from functional and structural connectivity. *Cereb Cortex*. 20:2636–2646.

Ullsperger M, Danielmeier C, Jocham G. 2014. Neurophysiology of performance monitoring and adaptive behavior. *Physiol Rev*. 94:35–79.

Ullsperger M, von Cramon DY. 2003. Error monitoring using external feedback: specific roles of the habenular complex, the reward system, and the cingulate motor area revealed by functional magnetic resonance imaging. *J Neurosci*. 23:4308–4314.

van Ede F, Quinn AJ, Woolrich MW, Nobre AC. 2018. Neural oscillations: sustained rhythms or transient burst-events? *Trends Neurosci*. 41:415–417.

Vidal J, Hamamé C, Jerbi K, Dalal S, Ciumas C, Perrone-Bertolotti M, Ossandon T, Minotti L, Kahane P, Lachaux J. 2011. Localizing cognitive functions in epilepsy with intracranial gamma-band dynamic responses introduction: complementing electrical cortical stimulation with a functional neural marker. In: *Neuropsychol Care People with Epilepsy Paris John Libbe*, pp. 324–334.

Voytek B, Kayser AS, Badre D, Fegen D, Chang EF, Crone NE, Parvizi J, Knight RT, D'Esposito M. 2015. Oscillatory dynamics coordinating human frontal networks in support of goal maintenance. *Nat Neurosci*. 18:1318–1324.

Wang X. 2010. Neurophysiological and computational principles of cortical rhythms in cognition. *Physiol Rev*. 90:1195–1268.

Watrous AJ, Deuker L, Fell J, Axmacher N. 2015. Phase-amplitude coupling supports phase coding in human ECoG. *elife*. 4:1–15.

Wessel JR, Danielmeier C, Morton JB, Ullsperger M. 2012. Surprise and error: common neuronal architecture for the processing of errors and novelty. *J Neurosci*. 32:7528–7537.

Zamorano F, Billeke P, Hurtado JM, López V, Carrasco X, Ossandón T, Aboitiz F. 2014. Temporal constraints of Behavioral inhibition: relevance of inter-stimulus interval in a go-Nogo task. *PLoS One*. 9:e87232.